Inclusive Λ^0 polarization in proton-nucleus collisions at 12 GeV

F. Abe, K. Hara,* S. Kim, K. Kondo, S. Miyashita, I. Nakano,
K. Takikawa, R. Tanaka,† Y. Yamamoto, T. Yasuda,‡ and K. Yasuoka§
Institute of Physics, University of Tsukuba, Sakura-mura, Ibaraki 305, Japan

Y. Asano and S. Mori
Institute of Applied Physics, University of Tsukuba, Sakura-mura, Ibaraki 305, Japan

Y. Fukui, S. Kurokawa, and A. Maki
National Laboratory for High Energy Physics (KEK), Oho-machi, Ibaraki 305, Japan
(Received 21 February 1986)

The polarization of Λ^0 hyperons in inclusive production by 12-GeV protons on nuclei has been measured for beryllium, copper, and tungsten targets. Data are obtained at five production angles, 3.5°, 5.0°, 6.5°, 8.0°, and 9.5°, covering the kinematic range $0.26 \leq x_F \leq 0.77$ and $0.4 \leq p_T \leq 1.5$ GeV/c. The dependence of the polarization on target nuclei is investigated by statistical analyses of the data. The polarization at fixed p_T increases roughly linearly with x_F. The present results are compared with other work at higher energies in terms of the A dependence and the (x_F, p_T) dependence.

I. INTRODUCTION

Recent studies of the polarization of Λ^0 hyperons in inclusive production by protons on nuclei have revealed that important spin effects exist in high-energy particle production.[1] Since the unexpected discovery[2] of substantial Λ^0 polarization at Fermilab, several experiments[3–9] have been performed at various laboratories, aiming at deeper understanding of the phenomena. The main results from these experiments can be summarized as follows. (1) The Λ^0 polarization is along the negative direction of the normal vector of the production plane. (2) The magnitude of the polarization increases monotonically with the transverse momentum p_T of the Λ^0, reaching to about 20% at $p_T = 1.5$ GeV/c. (3) The polarization increases with the Feynman scaling variable x_F as well as with p_T. (4) The polarization seems to depend weakly on the atomic mass of the target nucleus. (5) The polarization does not depend strongly on the energy of incident protons from 12 to 2000 GeV.

Information on the kinematic dependence of the polarization is essential to an understanding of the mechanism of inclusive Λ^0 polarization. In most of the early experiments the polarization was measured at one or a few fixed production angles. Since the x_F and p_T are mutually related at a fixed production angle, they were not able to separate the kinematic dependence of the polarization into the x_F dependence and the p_T dependence. To our knowledge, the data on the (x_F, p_T) dependence of the Λ^0 polarization come solely from the Fermilab experiments[1,8,9] at 400 GeV. In this paper we present the data on the (x_F, p_T) dependence at 12 GeV, which allow the comparison of the kinematic dependence of the Λ^0 polarization at different incident energies.

In the SU(6) quark model the spin of Λ^0 is identical to that of the s quark. The polarization of Λ^0's produced by the fragmentation of incident protons implies that the s quark produced in the reaction is polarized. Along with a growing body of experimental evidence, several theoretical models[10,11] have been proposed to explain the inclusive Λ^0 polarization by underlying constituent subprocesses. DeGrand and Miettinen[11] proposed a model based on the quark-recombination model. In their model, the polarization of quarks is due to the Thomas precession effect by a spin-orbit force in the recombination process of quarks, and the (x_F, p_T) dependence is predicted. The present data on the (x_F, p_T) dependence are compared with their model prediction.

Most of the early measurements on inclusive Λ^0 polarization were made on metal targets, such as Be, Ir, Pt, W, etc. The question of the A dependence (the dependence of the polarization on the atomic mass A of the target nucleus) was naturally raised. This was also stimulated by the results from the CERN ISR experiment,[5] which showed a larger polarization than the results from previous fixed-target experiments. The A dependence of Λ^0 polarization has been reported by Raychaudhuri *et al.*[6] for the incident energy of 28 GeV and by Heller *et al.*[9] for 400 GeV. Their results indicate that the magnitude of the polarization decreases with increasing A. As for the A dependence of hadron-production cross sections, extensive studies have been made[12] both experimentally and theoretically. The A dependence of Λ^0 polarization provides new information on hadron production off nuclei, independent of cross-section measurements.

In previous papers[7] we reported a measurement of Λ^0 polarization in inclusive production by 12-GeV protons on tungsten; the Λ^0's were observed to be polarized in roughly the same magnitude as observed at higher energies. In order to explore the A dependence and the kinematic dependence of the polarization in the 12-GeV energy region, we extended the measurement to beryllium and copper targets, and to five production angles: 3.5°, 5.0°, 6.5°, 8.0°, and 9.5°. The experimental setup was slightly

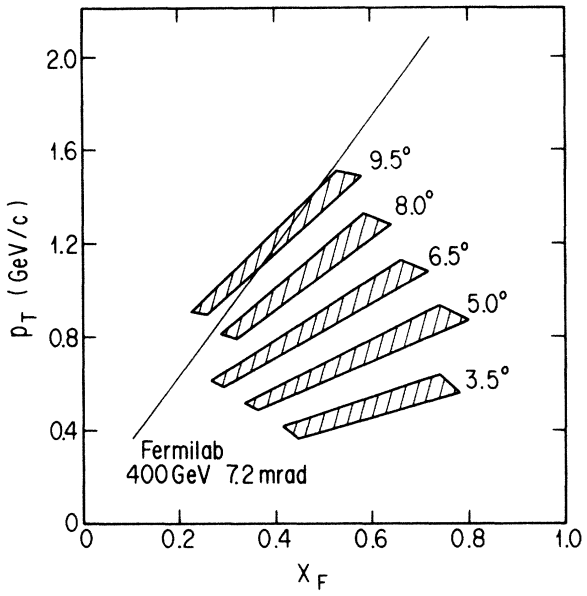

FIG. 1. The (x_F,p_T) plane. The hatched areas correspond to the kinematic regions covered by the present experiment. The solid line represents the kinematic region of data points in Ref. 4 for 400-GeV protons on Be at 7.2 mrad. The kinematic variables for $pA \rightarrow \Lambda^0 X$ are calculated on the assumption that the target is a proton at rest.

modified from the previous one[7] so as to be able to collect high-statistics data. The kinematic range covered is $0.26 \leq x_F \leq 0.77$ and $0.4 \leq p_T \leq 1.5$ GeV/c, as shown in Fig. 1. It should be noted that in the (x_F,p_T) plane our data points at 9.5° correspond to those of Heller *et al.*[4] for 400-GeV protons on Be at 7.2 mrad.

In this paper we present all the polarization data by 12-GeV protons on Be, Cu, and W at the five production angles, including the W data already published.[7] We describe the experimental apparatus in Sec. II and the data analysis in Sec. III. The polarization data are presented and discussed in Sec. IV. The A dependence is evaluated by statistical analyses of the data. The Cu and W data, after being corrected for small effects of the A dependence, are combined to the Be data. The (x_F,p_T) dependence of the combined data is compared with other data at higher energies.

II. EXPERIMENTAL APPARATUS

The experiment was performed in the EP2-A slow-extracted proton beam line of the KEK 12-GeV proton synchrotron. The beam line and the detectors were described previously.[7,13] The Λ^0's were produced by the primary proton beam on a metal target (30 mm wide $\times$ 10 mm high $\times$ 40 mm thick). They were extracted through a collimator with a solid angle of 100 μsr (10 mrad $\times$ 10 mrad). The Λ^0 production angle was defined by the collimator axis and the direction of the incident proton beam. It was varied in the range from 3.5° to 9.5° by steering the proton beam horizontally with two bending magnets placed upstream of the production target. The collimator was immersed in the vertical magnetic field of a sweeping magnet. The field integral of the sweeping magnet was 1.8 T m. The proton beam was focused on the target with a spot size of 6 mm in diameter (full width at half maximum). Typical beam intensities were 5×10^9 protons/pulse for 3.5° and 1.5×10^{10} protons/pulse for 9.5°; the beam pulse width was 0.5 s with a repetition period of 2.6 s.

The Λ^0's were identified by detecting the daughter protons and pions from the $\Lambda^0 \rightarrow p\pi^-$ decays. A schematic diagram of the apparatus is shown in Fig. 2. The apparatus consisted of two multiwire proportional chambers (PC1 and PC2), four multiwire drift chambers (DC1 to DC4), two spectrometer magnets (D1 and D2), scintillation counters (S1 to S5), scintillation hodoscope counters (HD1 and HD2), and a threshold gas Cherenkov counter.

Each of the tracking chambers consisted of four signal planes, X, Y, U, and V; the U,V wires were rotated by 45° with respect to the X,Y wires. The effective area of the proportional chamber PC1 was 40 cm $\times$ 40 cm, and that of PC2 was 92 cm $\times$ 92 cm. The wire spacing was 2 mm for both chambers. The effective area of the drift chambers DC1 and DC2 was 190 cm wide and 150 cm high, and they consisted of drift cells with a drift space of 2 cm. DC3 and DC4 had an effective area of 80 cm $\times$ 80 cm, and the drift space was 4 cm. The position resolutions (σ) were 250 μm for DC1 and DC2 and 350 μm for DC3 and DC4.

The pions were momentum analyzed by the first spectrometer magnet D1 and the protons by the second spectrometer magnet D2. D1 had an aperture 100 cm wide $\times$ 80 cm high with an iron length of 80 cm, and D2 was 60 cm wide, 40 cm high, and 100 cm long. The field distributions of D1 and D2 were measured with Hall probes

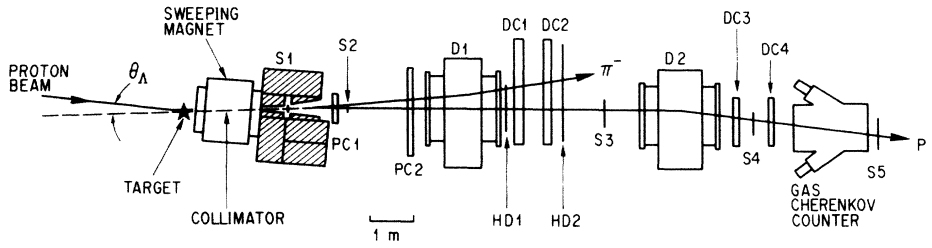

FIG. 2. Top view of the Λ^0 detection system. A typical event of the $\Lambda^0 \rightarrow p\pi^-$ decay is illustrated.

prior to the data-taking run. The three components of the magnetic field were measured at mesh points spaced at intervals of 5 cm. The field distribution was obtained by smoothing the measured values with use of the Laplace equation. The bending power of D1 averaged over the aperture was 0.521 T m and that of D2 was 1.266 T m.

The scintillation counter S1, placed at the exit of the collimator, was used to veto charged particles entering the decay region; the downstream end of the decay region was determined by the proportional chamber PC1. The counters S2 to S5 were placed along the path of the protons from the Λ^0 decays. Each of the hodoscope counters HD1 and HD2 was segmented horizontally into 16 elements. They were used to detect the pions as well as the protons. The threshold gas Cherenkov counter was used to distinguish between protons from the Λ^0 decays and pions from the K_s^0 decays. Freon 13 at atmospheric pressures was used as a radiator; the threshold momenta of Cherenkov radiation were 3.7 GeV/c for pions and 25 GeV/c for protons, respectively. Since the event rate of the K_s^0 decays turned out to be small, the Cherenkov counter was not incorporated into the event trigger, but used in the off-line analysis.

The event trigger was given by

$$T=S\bar{1}\cdot S2\cdot S3\cdot S4\cdot S5\cdot(\text{PC1 fast OR})\cdot\text{Hodo}\ ,$$

where the "PC1 fast OR" was formed from fast OR signals from the four planes of the proportional chamber PC1, each signal indicating the presence of wire hits in a plane. Two or more planes of PC1 were required to have wire hits. The "Hodo" was formed from a combination of signals from the hodoscope counters HD1 and HD2. Two-hit patterns characteristic of the $\Lambda^0\to p\pi^-$ decays were required for either of HD1 and HD2. The hit requirements of PC1 and the hodoscope counters were chosen to be loose in order to avoid possible biases in the trigger. This loose choice allowed the operating efficiencies of PC1, HD1, and HD2 to be monitored by the data from track reconstruction.

The experimental setup described above was modified from the previous one[7] in two major points. First, the polarity of the second spectrometer magnet D2 was reversed, and consequently the downstream drift chambers DC3 and DC4 were displaced from the collimator axis. Thus the neutral-particle background from the collimator did not bombard them in the present run. This allowed the operation of the apparatus at beam intensities 3 times higher than in the previous run. Second, with the addition of the hodoscope counter HD1 at the exit of the magnet D1, two-particle hits were required for the hodoscope counters as described above. The event trigger, which was a single-particle trigger in the previous run, was a two-particle trigger in the present run. This increased the rate of $\Lambda^0\to p\pi^-$ events contained in the triggers by 50%. These modifications altogether made it possible to collect data 4 times more efficiently than in the previous run.

The multiwire proportional chambers were read out by a serial data-transfer system,[14] and the multiwire drift chambers by the LeCroy DC201 amplifiers and 2770A digitizers. The data-acquisition system consisted of a mini-data processor Eclipse S/230 and a CAMAC branch-highway system.[7]

III. DATA ANALYSIS

A. Track reconstruction

The raw data were first processed by a hit-multiplicity selection routine in which the hit multiplicities of the tracking chambers were examined as to whether there were enough hits for two tracks to be reconstructed. The 24 planes of the tracking chambers were divided into three groups: zone 1 (PC1 and PC2), zone 2 (DC1 and DC2), and zone 3 (DC3 and DC4), each zone consisting of eight planes. A $\Lambda^0\to p\pi^-$ event has two tracks in zone 1 and zone 2, and one track in zone 3. In the hit-multiplicity selection routine we demanded that four or more planes out of the eight should have at least two hits in zone 1 and zone 2, and at least one hit in zone 3. About 55% of the triggers were rejected by this criterion. The left-right ambiguity of the drift chambers doubled the hit multiplicities in zone 2 and zone 3. The drift chambers also had a tendency to pick up accidental hits because of their long gate width; the gate widths were 0.6 μs for DC1 and DC2 and 1.0 μs for DC3 and DC4. Average hit multiplicities per event in zone 1, zone 2, and zone 3 were 2.2, 2×3.5, and 2×1.5, respectively.

In the track finding we first searched for a proton track, since it was localized in small areas of the chamber planes in zone 1 and zone 2 and was easier to find. Then the hits used for the proton track were removed, and a pion track was searched from the rest of the hits in the whole area of each chamber plane. An exception was $\Lambda^0\to p\pi^-$ events with small laboratory opening angles. In order to save these Λ^0's, events which had either the horizontal or the vertical projection of the proton track pointing back to the production target were retained as candidates for Λ^0's. They were reanalyzed in a separate track-finding routine.

A square-field approximation was used in the momentum reconstruction of tracks. The vertical deflection of tracks by the spectrometer magnets was small enough to allow the vertical projections of a track before and after the magnet to be fitted to a straight line. After the vertical projections of tracks were found, the horizontal projections were searched in each zone. A combination of tracks which had a minimum distance of separation at the middle of the spectrometer magnet was finally selected. The momentum was assigned based on a map of the bending powers $\int B\,dl$ of the spectrometer magnets. The bending power of D1 (D2) varied by 8% (1%) peak to peak over the entire aperture. In assigning momenta to the reconstructed pion and proton tracks, we used the average of three bending powers for incident positions of the particle at the entrance, middle, and exit of the magnet.

The proton track and the pion track in zone 1 were required to originate from a decay point in the decay region; the decay point was defined by a vertex point having the closest distance between the two tracks.

By using the reconstructed tracks, the chamber efficien-

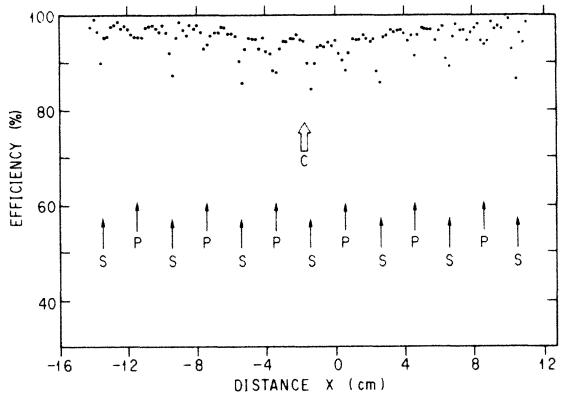

FIG. 3. Typical position dependence of the chamber efficiencies for the X plane of the drift chamber DC1. The arrows marked S and P indicate the positions of the sense wires and potential wires, respectively. The arrow marked C indicates the position on the axis of the collimator.

cies were calculated as a function of positions.[15] The chamber efficiencies decreased slightly around the supporting wires of PC2, and around the sense wires and the potential wires of the drift chambers. The drift cells of the drift chambers in the neutral-beam path had efficiencies a few percent lower compared with other cells because of the intense neutral-particle background. A typical position dependence of the drift-chamber efficiencies is shown in Fig. 3. These position dependences of the chamber efficiencies were taken into account in the polarization analysis (see subsection C). The position-averaged efficiencies of the chambers were 90—95%, depending on the chamber.

The efficiency of the track-finding program to reconstruct $\Lambda^0 \to p\pi^-$ events was evaluated as a function of the chamber efficiencies by a Monte Carlo simulation. In Fig. 4 we plot the dependence of the reconstruction efficiency on the chamber efficiencies, where all the chambers are assumed to have a common efficiency. Figure 4 shows that the reconstruction efficiency of the track-finding program is more than 90% for the operating chamber efficiencies.

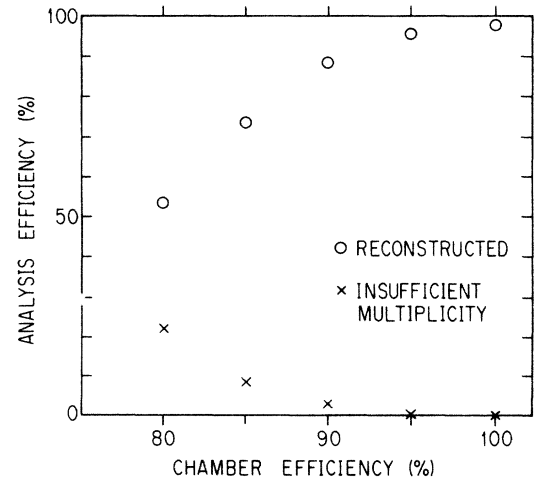

FIG. 4. Efficiencies of the track-reconstruction program as a function of the chamber efficiencies. The open circles denote the reconstruction efficiency and the crosses the fraction of events which are rejected by the hit-multiplicity selection routine.

B. Cuts

Several cuts were applied to the events which were selected by the track-reconstruction program. The momentum vector of the parent neutral particle reconstructed from the proton and pion tracks was traced back to the target, where a geometrical cut was applied. Events were rejected if the production point and the production angle were not within twice the boundary of the geometrical acceptance of the collimator. About 9% of the triggers were removed by this cut.

Conversions of photons $\gamma \to e^+e^-$ in the decay region showed a similar configuration of tracks as the $\Lambda^0 \to p\pi^-$ events with small opening angles, when the positrons were emitted with high momenta. In order to remove the γ contamination, the invariant mass was formed from the positive- and negative-charged particles for two hypotheses: $\Lambda^0 \to p\pi^-$ and $\gamma \to e^+e^-$. The γ's were well isolated from the Λ^0's in a scatter plot of the e^+e^- invariant mass versus the $p\pi^-$ invariant mass. About 5% of the triggers were identified as γ's and removed. The $K_s^0 \to \pi^+\pi^-$ backgrounds were investigated by using signals from the gas Cherenkov counter. The number of K_s^0's was less than 0.1% of the triggers.

Figure 5 shows a typical distribution of the resulting $p\pi^-$ invariant mass. The Λ^0 mass peak is formed with a resolution of $\sigma = 3.4$ MeV/c^2. Events within $\pm 3\sigma$ deviations from the mass peak were retained as the Λ^0 sample. About 30% of the triggers were identified as Λ^0's. The Λ^0 yields in empty-target runs were less than 2% of the target-in yields, and their contribution to the polarization values was negligible.

C. Polarization analysis

The Λ^0 polarization was determined from asymmetries in angular distributions of the decay products in the

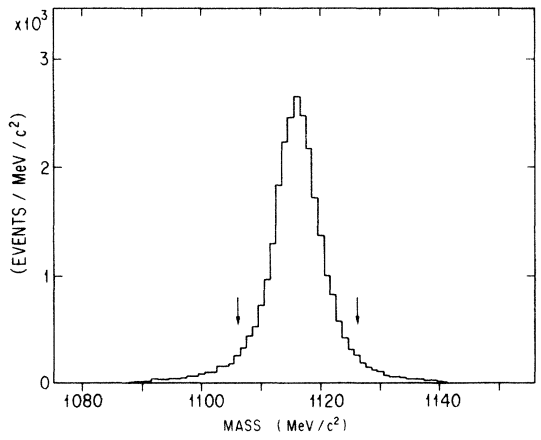

FIG. 5. Typical distribution of the $p\pi^-$ invariant mass. The arrows indicate the $\pm 3\sigma$ cuts.

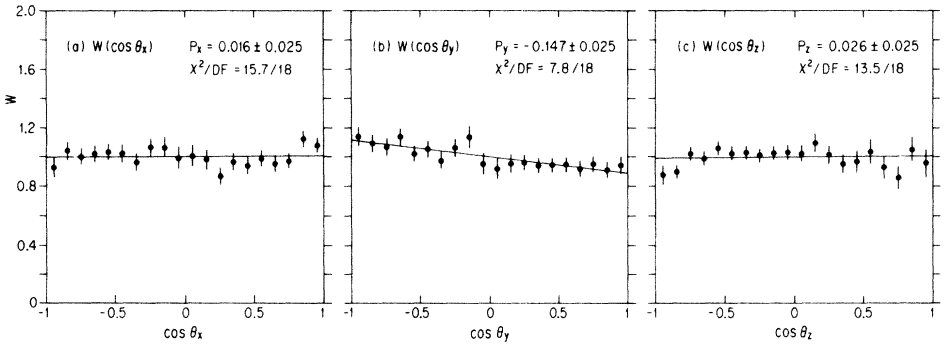

FIG. 6. Proton angular distributions $W(\cos\theta_i)$ corrected for the acceptance for the W data at $\theta=6.5°$ and $1.0\leq p_T\leq 1.1$ GeV/c: (a) events vs $\cos\theta_x$, (b) events vs $\cos\theta_y$, and (c) events vs $\cos\theta_z$. The solid lines are the straight-line fits to the data. The obtained polarization P_i ($i=x,y,z$) and χ^2 in the fitting are indicated.

$\Lambda^0\to p\pi^-$ decay. The following coordinate system was used in the polarization analysis: The y axis was normal to the production plane, and was defined by

$$\hat{\mathbf{n}}_y=\mathbf{p}_p\times\mathbf{p}_\Lambda/|\mathbf{p}_p\times\mathbf{p}_\Lambda|\ ,$$

where $\mathbf{p}_p$ was the momentum vector of the beam proton, and $\mathbf{p}_\Lambda$ was that of the reconstructed Λ^0. The z axis was along the direction of motion of the Λ^0, $\hat{\mathbf{n}}_z=\mathbf{p}_\Lambda/|\mathbf{p}_\Lambda|$. The x axis was defined by $\hat{\mathbf{n}}_x=\hat{\mathbf{n}}_y\times\hat{\mathbf{n}}_z$. In the rest frame of the Λ^0, the angular distribution of the daughter proton from the $\Lambda^0\to p\pi^-$ decay is given by

$$\frac{dN}{d\cos\theta_i}=\tfrac{1}{2}A(\cos\theta_i)(1+\alpha P_i\cos\theta_i),\quad i=x,y,z\ , \qquad (1)$$

where $\mathbf{P}$ (P_x,P_y,P_z) is the polarization vector of the Λ^0, α is the analyzing power for the $\Lambda^0\to p\pi^-$ decay ($\alpha=0.642\pm0.013$ from Ref. 16), $\cos\theta_i$ is the direction cosine of the proton, i.e., $\cos\theta_i=\hat{\mathbf{k}}\cdot\hat{\mathbf{n}}_i$ with $\hat{\mathbf{k}}$ denoting the direction vector of the proton, and $A(\cos\theta_i)$ is an acceptance of the detection system. The polarization component P_x corresponds to a left-right decay asymmetry, the P_y an up-down asymmetry, and the P_z a forward-backward asymmetry. The acceptance $A(\cos\theta_i)$ depends on other variables as well, e.g., the momentum of the Λ^0, the decay point of the Λ^0, and detection efficiencies for the daughter particles.

The acceptance was calculated by a hybrid Monte Carlo technique.[17] The basic idea in the hybrid Monte Carlo technique is to simulate variables in an experiment which are important to the physical result of interest, and to use real data for other variables which are spectators in the result. In our case, Monte Carlo events were generated for each of the real events to calculate the acceptance $A(\cos\theta_i)$, in which we used the decay point and the laboratory momentum of the Λ^0 as determined from the measurements, with the polarization P_i set equal to zero. The event generation was repeated until ten Monte Carlo events were accepted for each real event. The angular distribution of the daughter protons corrected for the acceptance was fitted to a straight line, and the slope αP_i was determined (see Fig. 6).

The position-dependent efficiencies of the tracking chambers were taken into account in the Monte Carlo simulation in the following way. (1) The daughter protons and pions were traced through the experimental setup, and hit positions on the chambers were calculated. Effects due to multiple scattering, energy loss, and pion decay in flight were included in the tracing. (2) Chamber hits were generated according to the chamber efficiencies at incident positions of the particles. (3) An event was regarded as being detected if the generated hit multiplicities satisfied the criterion imposed on real data in the hit-multiplicity selection routine of the track-finding program. This correction was essential to reproduce various distributions of the daughter protons and pions, such as the laboratory-momentum distributions and the hit-position distributions. As an example, Fig. 7 shows measured and calculated hit-position distributions of the protons on the X plane of the drift chamber DC2. The Monte Carlo simulation reproduces the real data well.

According to parity conservation in strong interactions, the polarization vector should be normal to the production plane.[18] In our experimental setup, the normal of the

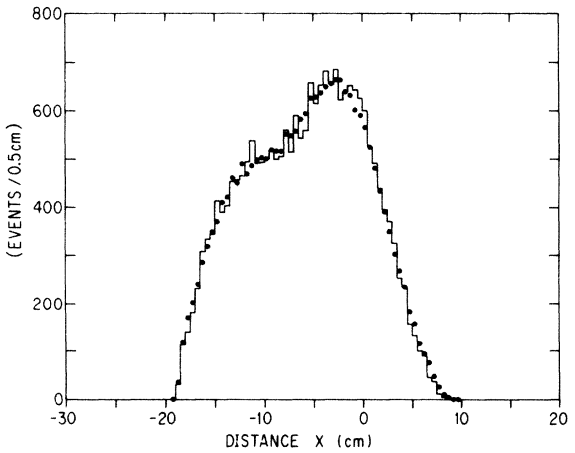

FIG. 7. Typical distribution of the daughter protons on the X plane of the drift chamber DC2. The distribution of measured events is shown by solid lines and that of the Monte Carlo simulation by solid circles.

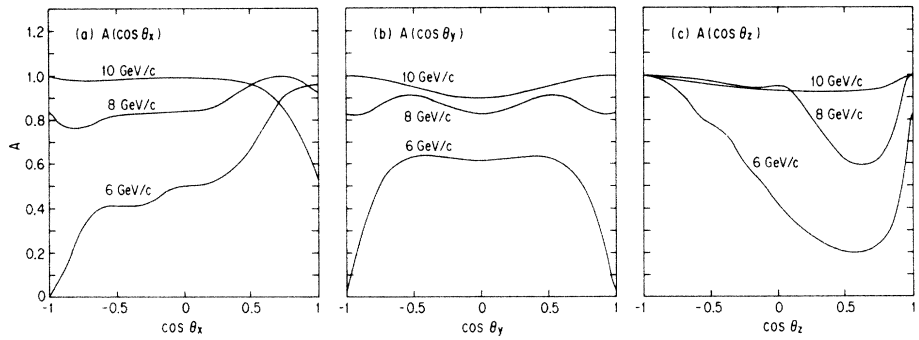

FIG. 8. The geometrical acceptance $A(\cos\theta_i)$ for the Λ^0 momenta of 6, 8, and 10 GeV/c: (a) A vs $\cos\theta_x$, (b) A vs $\cos\theta_y$, and (c) A vs $\cos\theta_z$.

production plane $\hat{\mathbf{n}}_y$ was essentially vertical, and the magnetic field of the sweeping magnet was also vertical. Effects of spin precession in the sweeping magnet were negligibly small. Hence the Λ^0's in the decay region should have $P_x=P_z=0$. Measurements of the P_x were used to estimate systematic biases in the present results of the polarization of the Λ^0, P_y. The P_z was not used because it was sensitive to small variations in the acceptance correction and the momentum determination of the daughter particles. The P_x and P_y were insensitive to those variations. This P_z difficulty originated from a strong forward-backward asymmetry of the acceptance $A(\cos\theta_z)$ at lower momenta of the Λ^0. Figure 8 shows the geometrical acceptances as a function of $\cos\theta_i$ ($i=x,y,z$) for three typical momenta of the Λ^0, 6, 8, and 10 GeV/c. The $A(\cos\theta_z)$ was a rapidly varying function of $\cos\theta_z$ at lower momenta of Λ^0's, while the $A(\cos\theta_x)$ and $A(\cos\theta_y)$ varied more slowly than the $A(\cos\theta_z)$.

The average values of P_x were -0.017 ± 0.005 for Be, -0.008 ± 0.004 for Cu, and -0.021 ± 0.004 for W. Nonzero values of P_x could be ascribed to small errors in the Monte Carlo correction for the chamber efficiencies. As described in Sec. III A, the drift chambers had lower efficiencies in those areas which were exposed to the intense neutral-beam background. Protons striking these areas corresponded to positive values of $\cos\theta_x$ in the angular distribution in the Λ^0 rest frame. Small errors in the chamber-efficiency correction could therefore give asymmetries in the $\cos\theta_x$ distribution and spurious polarization values of P_x. On the other hand, the experimental setup was designed to be up-down symmetric. In the $\cos\theta_y$ distribution the protons striking the chamber areas with lower efficiencies were distributed symmetrically around $\cos\theta_y=0$. Hence the effects of errors in the chamber-efficiency correction on P_y were smaller than those on P_x. From the measured values of P_x and the above considerations, we estimated the systematic bias in the polarization values of P_y to be less than 2%.

IV. RESULTS AND DISCUSSION

Data were collected at five production angles, 3.5°, 5.0°, 6.5°, 8.0°, and 9.5°, for three target nuclei, Be ($A=9.0$), Cu ($A=63.5$), and W ($A=183.9$). The numbers of Λ^0's accumulated for Be, Cu, and W targets were 6.0×10^5, 8.7×10^5, and 1.2×10^6, respectively. Table I lists the numerical values of the polarization $P_\Lambda=P_y$. The quoted errors are statistical only. The W data at 3.5° and the Be,Cu data at 3.5°,6.5° were taken by the old setup described previously.[7] One-half of the W data at 6.5° and 9.5° were taken by the old setup, and the other half by the new setup described in this paper. Comparison between the two sets of the data showed a good agreement within statistical accuracies. They were therefore combined, and the combined values are listed in Table I. Other data in Table I were taken by the new setup.

A. A dependence

The polarizations P_Λ for Be, Cu, and W targets are plotted in Fig. 9 as a function of p_T at fixed production angles. As shown in the figure, the polarizations are roughly equal for the three targets. We made a χ^2 test to examine whether these polarizations had any significant A dependence. To that end, the W data at each production angle were divided into p_T bins at intervals of $\Delta p_T=0.1$ GeV/c, and were fitted to a straight line. The obtained straight lines are also shown in Fig. 9. The total χ^2 value in the fitting, summed over five production angles, was 17.0 for 12 degrees of freedom. We then calculated χ^2's for the hypothesis that the p_T dependences of the Be and Cu data at each production angle were described by the same function as determined for W. The obtained χ^2 values were 37.5 for 22 data points for Be and 22.7 for 22 data points for Cu. Hence the polarization data for Cu have essentially the same p_T dependence as for W. On the other hand, the Be data seem to have a different p_T dependence as compared with the W data.

In order to investigate the differences or similarities between the Be, Cu, and W data in more detail, we plot in Fig. 10 distributions of the residuals of the polarization data, $(P_{\Lambda i}-f^{\mathrm{W}})/\sigma_i$, where $P_{\Lambda i}$ are the polarization data for Be, Cu, and W at a given production angle and p_T, f^{W} is the corresponding value of the linear function fitted to the W data, and σ_i are the statistical errors of $P_{\Lambda i}$. Figure 10 shows that the distribution of the residuals of the Cu data is roughly similar to that of the W data, while the Be data points are distributed more frequently in negative residuals than in positive ones. This suggests that, on the average, the polarization for Cu is essentially the same as

TABLE I. Λ^0 polarization on W, Cu, and Be targets at production angles 3.5°, 5.0°, 6.5°, 8.0°, and 9.5°. The combined polarization is also shown. $\bar{x}_F$ denotes the mean value of x_F corresponding to the p_T bin at each production angle.

Angle (deg)	p_T (GeV/c)	$\bar{x}_F$	P_Λ (%) W	Cu	Be	Combined
3.5	0.4–0.5	0.57	−8.2±2.2	−7.4±1.4	−6.2±1.6	−7.7±1.1
	0.5–0.6	0.71	−5.1±2.2	−6.2±1.3	−9.1±1.7	−7.7±1.0
5.0	0.5–0.6	0.40	−9.1±2.7	−2.7±2.4	−1.9±2.9	−4.9±1.7
	0.6–0.7	0.51	−9.7±2.0	−9.0±1.8	−12.0±2.1	−11.2±1.3
	0.7–0.8	0.62	−12.7±2.0	−11.5±1.8	−13.6±2.1	−13.8±1.3
	0.8–0.9	0.72	−14.0±2.5	−14.0±2.4	−21.0±2.7	−17.9±1.6
6.5	0.6–0.7	0.35	−7.9±2.1	−9.9±2.9	−7.8±2.9	−9.1±1.6
	0.7–0.8	0.43	−15.8±1.4	−9.7±1.9	−11.4±1.9	−13.9±1.1
	0.8–0.9	0.51	−12.8±1.2	−11.8±1.7	−15.7±1.7	−14.7±1.0
	0.9–1.0	0.59	−15.3±1.3	−15.2±1.8	−18.6±1.8	−17.8±1.1
	1.0–1.1	0.66	−16.7±1.7	−16.4±2.4	−25.0±3.0	−20.4±1.5
8.0	0.8–0.9	0.34	−4.2±3.2	−10.8±3.6	−8.9±3.9	−8.3±2.2
	0.9–1.0	0.40	−10.7±2.8	−8.6±3.1	−12.9±3.3	−11.8±1.9
	1.0–1.1	0.47	−13.1±2.7	−14.0±3.1	−13.7±3.3	−14.8±1.9
	1.1–1.2	0.53	−15.4±3.1	−18.3±3.4	−23.4±3.7	−20.6±2.2
	1.2–1.3	0.59	−24.4±3.9	−22.3±4.4	−21.6±4.8	−25.0±2.8
9.5	0.9–1.0	0.29	−10.1±2.3	−10.1±2.2	−7.7±3.5	−10.7±1.7
	1.0–1.1	0.34	−11.4±1.9	−14.5±1.9	−14.8±3.0	−14.7±1.4
	1.1–1.2	0.39	−14.5±1.9	−16.5±1.8	−16.3±2.9	−17.4±1.4
	1.2–1.3	0.44	−18.8±1.9	−17.0±1.9	−15.1±3.1	−19.3±1.5
	1.3–1.4	0.49	−14.5±2.2	−17.1±2.2	−18.0±3.7	−18.0±1.7
	1.4–1.5	0.54	−19.3±2.6	−13.7±2.9	−17.2±4.8	−18.8±2.1

for W, and the polarization for Be is slightly larger in magnitude than that for W.

A quantitative estimation of the difference between the Be, Cu, and W data was made in the following way. We assumed that the p_T dependence of the polarizations at a fixed production angle was given by a single functional form, independent of target nuclei, and that the A dependence consisted of the difference in an overall multiplicative coefficient. To be more specific, on the assumption that the polarization for Be or Cu was different from the polarization for W by a constant factor K, we investigated if the differences $P_{\Lambda i}-KP^{\mathrm{W}}_{\Lambda i}$ were consistent with zero statistically, where i runs over the data points, $P^{\mathrm{W}}_{\Lambda i}$ is the polarization data for W at the ith data point, and $P_{\Lambda i}$ is the corresponding data for Be or Cu. The constant factor K was determined by minimizing the χ^2:

$$\chi^2=\sum_i \frac{(P_{\Lambda i}-KP^{\mathrm{W}}_{\Lambda i})^2}{(\sigma_i)^2+(K\sigma^{\mathrm{W}}_i)^2}\ , \tag{2}$$

where σ_i (σ^{W}_i) are the statistical errors of the data $P_{\Lambda i}$ ($P^{\mathrm{W}}_{\Lambda i}$). The obtained K factors and χ^2 divided by the number of degrees of freedom, χ^2/DF, are

$$K=1.12\pm0.05 \quad \text{with } \chi^2/\mathrm{DF}=24.8/21 \quad \text{for Be}\ , \tag{3a}$$

$$K=0.96\pm0.05 \quad \text{with } \chi^2/\mathrm{DF}=17.2/21 \quad \text{for Cu}\ . \tag{3b}$$

The χ^2 values in Eqs. (3) support the initial assumption that the A dependence of our data can be parametrized by a single constant factor K. The obtained values of K seem to indicate that the Λ^0 polarization on Be is about 10% higher than that on Cu and W, although the statistical significance is marginal. The previous data[6] at 28 GeV and the data[1,9] at 400 GeV indicate a trend that the Λ^0 polarization decreases with increasing A. The present results at 12 GeV are compatible with the trend observed at higher energies.

B. Kinematic dependence

In order to investigate the kinematic dependence of the polarization with better statistics, we combined the Cu and W data with the Be data, taking into account the K factors given in Eqs. (3). The combined polarization is normalized to that on Be. The numerical values of the combined polarization are listed in Table I. Figure 11 shows the combined polarization as a function of p_T at fixed production angles. Also shown are the data of Heller *et al.*[4] for 400-GeV protons on Be at 7.2 mrad. Our data at 9.5° agree with their data well. As mentioned in Sec. I, our data points at 9.5° overlap with their data points in the (x_F,p_T) plane. The agreement between the two data demonstrates that the Λ^0 polarization, when compared at the same x_F and p_T, does not depend on the energy of incident protons from 12 to 400 GeV.

Figure 12 shows the combined polarization as a function of x_F at fixed p_T. Our data indicate that the magni-

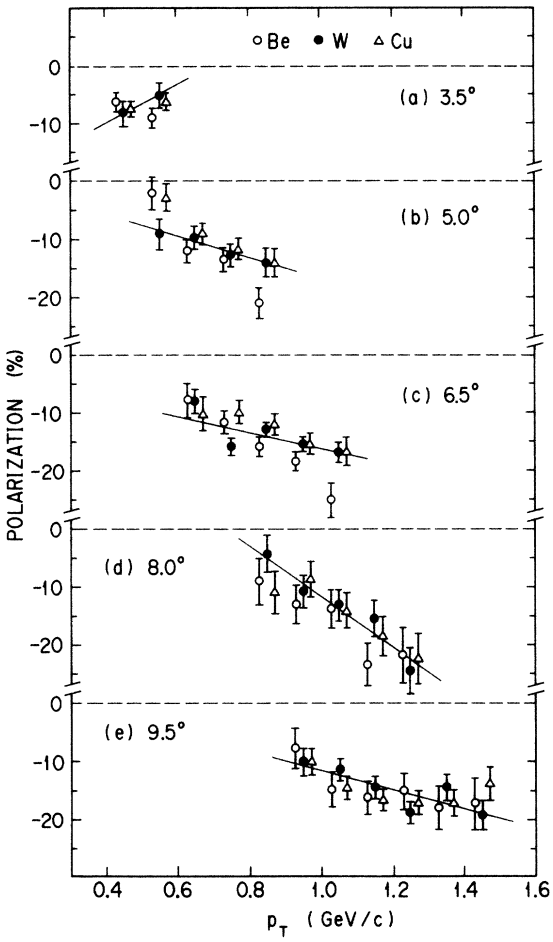

FIG. 9. Λ^0 polarization by 12-GeV protons on Be, Cu, and W as a function of p_T at fixed production angles: (a) 3.5°, (b) 5.0°, (c) 6.5°, (d) 8.0°, and (e) 9.5°. The W data (solid circles) are plotted at correct p_T values; the Be data (open circles) and Cu data (open triangles) are plotted at slightly displaced p_T values. The solid lines are linear fits to the W data points.

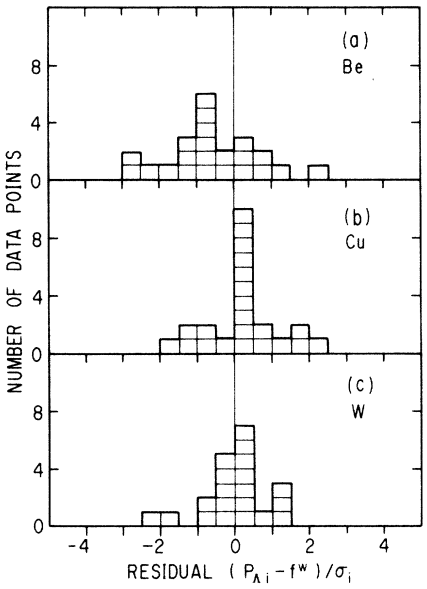

FIG. 10. Distributions of the residuals $(P_{\Lambda i}-f^W)/\sigma_i$ for (a) Be, (b) Cu, and (c) W, where $P_{\Lambda i}$ are the polarization data for Be, Cu, and W at a given production angle and p_T, σ_i are the errors of $P_{\Lambda i}$, and f^W is the linear fit to the W data.

tude of the Λ^0 polarization increases with x_F in the range $0.3 \leq x_F \leq 0.7$. Earlier experiments presumably were not able to separate the x_F dependence from the p_T dependence, either because of limited statistics or because the kinematic range covered was small. Recent experiments[1,8,9] at Fermilab report the x_F dependence at 400 GeV. As demonstrated in Fig. 11, the present results on the (x_F,p_T) dependence are consistent with the data at 400 GeV, indicating that the Λ^0 polarization as a function of x_F and p_T scales from 12 to 400 GeV.

Solid curves in Fig. 12 are calculated by the model of DeGrand and Miettinen,[11] which ascribes the polarization to Thomas precession effects in the quark-recombination process. At $p_T \lesssim 1.0$ GeV/c, the model prediction agrees fairly well with the present data. At $p_T \gtrsim 1.0$ GeV/c, however, the data are larger than the model prediction by about 5% in magnitude of the polarization.

We know of no theory which can predict both of the (x_F,p_T) dependence and the A dependence of the Λ^0 polarization. A qualitative argument is given by Pondrom.[1]

One of the successful pictures of hadron production off nuclei is the projectile straggling model.[19] The basic idea of the model is that the momenta of the valence and sea quarks of the projectile proton are degraded as they go through the nucleus. At high energies the degraded quarks recombine into the Λ^0 outside the nucleus. Since the Λ^0 polarization increases monotonically with increas-

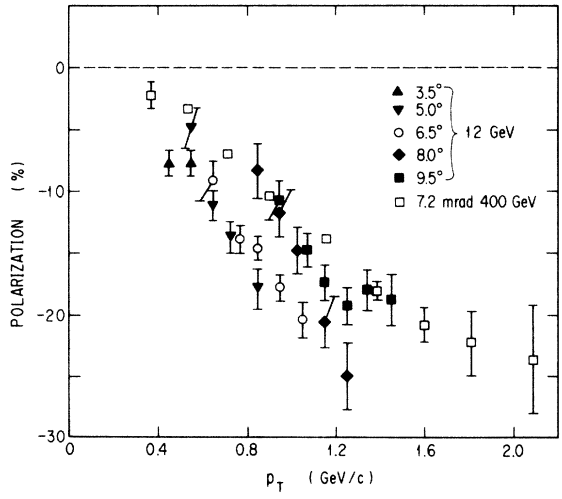

FIG. 11. Combined polarization as a function of p_T at fixed production angles. The error bars of the 12-GeV data are statistical only; the systematic uncertainty is estimated to be less than 2%. The data at 400 GeV (Ref. 4) are shown for comparison.

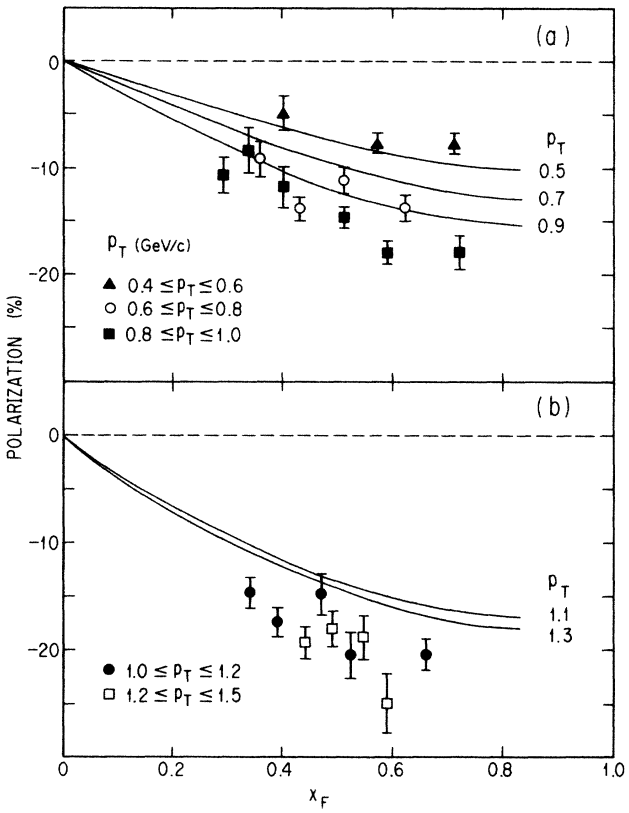

FIG. 12. Combined polarization as a function of x_F at fixed p_T: (a) for $0.4 \leq p_T \leq 1.0$ GeV/c and (b) for $1.0 \leq p_T \leq 1.5$ GeV/c. The error bars are statistical only; the systematic uncertainty is estimated to be less than 2%. The curves are the predictions of the Thomas precession model (Ref. 11).

ing x_F, and since straggling in a heavy nucleus shifts high x_F to lower x_F, the Λ^0 polarization at a given x_F value would increase in a heavy nucleus, unless the straggling is accompanied by some depolarization mechanism which overcompensates for the shift in x_F. The observed trend that the magnitude of the polarization is smaller in heavier nuclei implies the presence of some depolarization mechanism in the straggling. We note that the above argument tacitly assumes that the s quark is polarized when created. If the s quark gets polarized in the quark-recombination process, which occurs outside the nucleus, the Λ^0 polarization at a given x_F value would not depend on A. Thus the A dependence is related to a basic problem as to when the s quark gets polarized in space-time development of Λ^0 production off nuclei. In view of the limited statistical significance of our results on the A dependence, more experimental study is needed to help deeper understanding of the phenomena.

V. CONCLUSIONS

We have measured the Λ^0 polarization in inclusive production by 12-GeV protons on Be, Cu, and W targets. The kinematic range was $0.26 \leq x_F \leq 0.77$ and $0.4 \leq p_T \leq 1.5$ GeV/c. The main conclusions are as follows.

(1) The polarization on Be seems to be slightly larger in magnitude than that on Cu and W, although the statistical significance is marginal.

(2) The magnitude of the polarization at fixed p_T increases roughly linearly with x_F.

(3) The (x_F, p_T) dependence of the polarization is in qualitative agreement with the Thomas precession model[11] at lower p_T ($\lesssim 1$ GeV/c). At higher p_T ($\gtrsim 1$ GeV/c), the data show larger polarizations than the model predicts.

(4) The (x_F, p_T) dependence of the polarization is consistent with the data[1,8,9] at 400 GeV, indicating the scaling of the Λ^0 polarization from 400 GeV down to 12 GeV.

ACKNOWLEDGMENTS

This experiment would not have been possible without the encouragement provided by Professor T. Nishikawa, Professor S. Suwa, Professor S. Ozaki, and Professor A. Kusumegi. Many people have contributed to the success of the experiment. We wish to thank members of the KEK beam channel group for their aid in constructing and operating the Λ^0 beam line. We wish to thank members of the 12-GeV proton synchrotron division for their efficient operation of the accelerator. The gas Cherenkov counter was constructed by members of the KEK machine shop, to whom we wish to express our appreciation. We also wish to thank members of the KEK data-handling division for their kind help in the data analysis. We wish to especially thank Professor L. G. Pondrom for valuable discussions.

*Present address: Institute of Physics, University of Berne, Sidlerstrasse 5, 3012 Berne, Switzerland.

†Present address: Department of Physics, Chuo University, Kasuga, Bunkyo-ku, Tokyo 112, Japan.

‡Present address: Physics Department, Northeastern University, 360 Huntington Ave., Boston, MA 02215.

§Present address: Fermi National Accelerator Laboratory, P.O. Box 500, Batavia, IL 60510.

[1]For a recent review of hyperon production, see L. G. Pondrom, Phys. Rep. **122C**, 57 (1985).

[2]G. Bunce *et al.*, Phys. Rev. Lett. **36**, 1113 (1976).

[3]K. Heller *et al.*, Phys. Lett. **68B**, 480 (1977); F. Lomanno *et al.*, Phys. Rev. Lett. **43**, 1905 (1979).

[4]K. Heller *et al.*, Phys. Rev. Lett. **41**, 607 (1978); **45**, 1043(E) (1980).

[5]S. Erhan *et al.*, Phys. Lett. **82B**, 1325 (1979).

[6]K. Raychaudhuri *et al.*, Phys. Lett. **90B**, 319 (1980); **93B**, 525(E) (1980).

[7]F. Abe *et al.*, Phys. Rev. Lett. **50**, 1102 (1983); F. Abe *et al.*, J. Phys. Soc. Jpn. **52**, 4107 (1983).

[8]K. Heller, in *High Energy Physics—1980,* edited by L. Durand and L. Pondrom (AIP Conf. Proc. No. 68) (AIP, New York, 1981), p. 61; B. Lundberg *et al.*, in *High Energy Spin Physics—1982,* edited by G. M. Bunce (AIP Conf. Proc. No.

95) (AIP, New York, 1983), p. 83; K. Heller, in *Proceedings of the 6th International Symposium on High Energy Spin Physics,* Marseille, France, 1984, edited by J. Soffer [J. Phys. (Paris) Colloq. **46**, C2-121 (1985)].

[9]K. Heller *et al.*, Phys. Rev. Lett. **51**, 2025 (1983).

[10]K. Heller *et al.*, in Ref. 4; B. Andersson, G. Gustafson, and G. Ingelman, Phys. Lett. **85B**, 417 (1979); J. Szwed, *ibid.* **105B**, 403 (1981); R. Lednicky, Z. Phys. C **26**, 531 (1985).

[11]T. DeGrand and H. Miettinen, Phys. Rev. D **23**, 1227 (1981); **24**, 2419 (1981); **31**, 661(E) (1985).

[12]See, for example, A. Białas, in *Multiparticle Dynamics 1982,* proceedings of the XIIIth International Symposium, Volendam, The Netherlands, edited by E. W. Kittel, W. Metzger, and A. Stergiou (World Scientific, Singapore, 1983), pp. 328–358; see also L. G. Pondrom in Ref. 1.

[13]F. Abe *et al.*, Nucl. Instrum. Methods **220**, 293 (1984).

[14]S. Dhawan, IEEE Trans. Nucl. Sci. **NS-21**, 922 (1974); S. Dhawan, K. Kondo, K. Takikawa, and K. Yasuoka, Jpn. J. Appl. Phys. **23**, 492 (1984).

[15]The efficiencies of the trigger counters were also measured from the reconstructed tracks regularly during the data-taking runs, and they were sufficiently high (greater than 99%).

[16]M. Roos *et al.* (Particle Data Group), Phys. Lett. **111B**, 1 (1982).

[17]G. Bunce, Nucl. Instrum. Methods **172**, 553 (1980).

[18]That the polarization is indeed normal to the production plane has been established by other experiments; see, for example, G. Bunce *et al.* in Ref. 2 and K. Heller *et al.* in Ref. 3.

[19]K. Heller *et al.*, Phys. Rev. D **16**, 2737 (1977); B. Durand and J. Krebs, *ibid.* **21**, 3137 (1980); R. C. Hwa, Phys. Rev. Lett. **52**, 492 (1984).